Received: June 8, 2023 Revised: August 11, 2023 Accepted: September 12, 2023

https://doi.org/10.1016/j.neurom.2023.09.003

# Seeing Is Believing: Photon Counting Computed Tomography Clearly Images Directional Deep Brain Stimulation Lead Segments and Markers After Implantation

James Manfield, MSc[1]; Sheena Thomas, BSc[2]; Marko Bogdanovic, MD[1]; Nagaraja Sarangmat, MBBS[1]; Charalambos Antoniades, PhD[2]; Alexander L. Green, PhD[1,3]; James J. FitzGerald, PhD[1,3]

## ABSTRACT

**Background and Objectives:** Directional deep brain stimulation (DBS) electrodes are increasingly used, but conventional computed tomography (CT) is unable to directly image segmented contacts owing to physics-based resolution constraints. Postoperative electrode segment orientation assessment is necessary because of the possibility of significant deviation during or immediately after insertion. Photon-counting detector (PCD) CT is a relatively novel technology that enables high resolution imaging while addressing several limitations intrinsic to CT. We show how PCD CT can enable clear in vivo imaging of DBS electrodes, including segmented contacts and markers for all major lead manufacturers.

**Materials and Methods:** We describe postoperative imaging and reconstruction protocols we have developed to enable optimal lead visualization. PCD CT images were obtained of directional leads from the three major manufacturers and fused with preoperative 3T magnetic resonance imaging (MRI). Radiation dosimetry also was evaluated and compared with conventional imaging controls. Orientation estimates from directly imaged leads were compared with validated software-based reconstructions (derived from standard CT imaging artifact analysis) to quantify congruence in alignment and directional orientation.

**Results:** High-fidelity images were obtained for 15 patients, clearly indicating the segmented contacts and directional markers both on CT alone and when fused to MRI. Our routine imaging protocol is described. Ionizing radiation doses were significantly lower than with conventional CT. For most leads, the directly imaged lead orientations and depths corresponded closely to those predicted by CT artifact-based reconstructions. However, unlike direct imaging, the software reconstructions were susceptible to 180° error in orientation assessment.

**Conclusions:** High-resolution photon-counting CT can very clearly image segmented DBS electrode contacts and directional markers and unambiguously determine lead orientation, with lower radiation than in conventional imaging. This obviates the need for further imaging and may facilitate anatomically tailored directional programming.

**Keywords:** Deep brain stimulation, directional electrodes, imaging, orientation, photon-counting CT

## INTRODUCTION

Directional deep brain stimulation (DBS) leads have been rapidly adopted and are in widespread use worldwide. Their principal benefit is the improvement offered in therapeutic window through customization of the electrical field shape, for which class I evidence now exists.[1,2] There also may be a reduction in energy consumption[3] with a commensurate increase in implanted pulse generator (IPG) longevity.[4]

The price paid for this flexibility is a substantial increase in programming complexity. With the current de facto standard 1-3-3-1 configuration (comprising two levels of three-segment contacts sandwiched between two complete ring electrodes), it is estimated that programming time may be tripled compared with

Address correspondence to: James J. FitzGerald, PhD, Nuffield Department of Surgical Sciences, University of Oxford, Oxford, UK. Email: james.fitzgerald@nds.ox.ac.uk

[1] Oxford Functional Neurosurgery, John Radcliffe Hospital, Oxford, UK;
[2] Radcliffe Department of Medicine, University of Oxford, Oxford, UK; and
[3] Nuffield Department of Surgical Sciences, University of Oxford, Oxford, UK

For more information on author guidelines, an explanation of our peer review process, and conflict of interest informed consent policies, please see the journal's Guide for Authors.

Source(s) of financial support: This work was supported by the Oxford Biomedical Research Centre through the Surgical, Cardiac and Imaging themes.

nondirectional leads.[5,6] An accurate postoperative estimation of lead orientation is essential to efficient setup, given this often shifts periinsertion[3,7,8] but remains stable thereafter.[9]

The limited resolution of current computed tomography (CT) scanners has prevented direct imaging of lead segments. Various approaches to orientation detection have been adopted, including two-plane fluoroscopy, rotational fluoroscopy, and methods based on analysis of CT artifact.[10–12]

The first production CT scanner was installed at Atkinson Morley hospital, London, UK, over 50 years ago. There have since been several major advances, including spiral CT, multislice CT, and dual energy CT. However, the fundamental detector technology has remained similar. In a conventional CT detector (Fig. 1a), x-ray photons that have passed through the patient enter a scintillator, typically a layer of gadolinium oxysulphide or thallium-doped caesium iodide. Within this material, the x-rays cause release of visible photons. Some of these continue to a photodiode layer underneath the scintillator, where they cause a current to flow, known as the photocurrent. The photocurrent from each element of the photodiode array forms the information from which the image is computed. This is an analog device: The current from each photodiode reflects the total x-ray energy incident on the area of scintillator above it.

The image quality and resolution of conventional CT are limited by several factors. The photocurrent is small, and there is an electrical noise current added to the signal coming from each photodiode, which degrades image quality. Increasing the x-ray dose increases the photocurrent level and thus signal to noise ratio (SNR) but is clearly undesirable from a safety point of view. Resolution is limited partly by similar considerations—reducing the size of each photodiode in the array would reduce the photocurrent coming from each element,[13] necessitating an increase in dose to maintain SNR. Furthermore, the visible photons produced in the scintillator are scattered in many directions, and to prevent resolution being degraded owing to their lateral spread, the photodiode array must contain septa. These occupy space, which also limits resolution.

Photon counting detectors (PCDs) (Fig. 1b) dispense with the scintillator; x-rays instead pass into a semiconductor (cadmium telluride), where they cause release of electrons. These electrons are swept in one direction by an applied electric field to a pixelated anode, and septa are not needed. Each burst of electrons released by an x-ray photon causes a discrete current pulse from the relevant anode segment. The pulses in each interval are counted, and the total is the information used to form the image; this is the digital equivalent of the analog photocurrent in a conventional detector. Importantly, the size of the pulse from each absorbed x-ray photon is large compared with the noise amplitude; thus, noise may be substantially decreased by only counting pulses that exceed a certain threshold, and in many applications, dose may be reduced. Reducing element size does not affect the current generated per photon, and resolution may therefore be greatly increased.[14,15]

The highest resolution offered by PCD CT is now 0.11 mm, some two to four times finer than that of contemporary conventional CT.[16,17] This, coupled with the low noise inherent in the system and potential for reduced radiation dose, led us to use PCD CT routinely for postoperative CT imaging of patients having DBS. The technology is approved for routine diagnostic use and reliably excludes hematoma, which is one of the purposes of postoperative imaging in DBS. The objective of this article is to illustrate the capabilities of PCD CT in directional DBS lead imaging compared with existing technologies, provide parameters to enable reproduction, and evaluate the dose reduction achieved compared with our previous standard postoperative imaging approach in patients with directional leads—namely, a conventional CT scan followed by orthogonal fluoroscopic views of the orientation marker.

## MATERIALS AND METHODS

Fifteen patients underwent postoperative imaging after DBS insertion. Their diagnoses, stimulation targets, and the lead models inserted are listed in Table 1. Leads were manufactured by

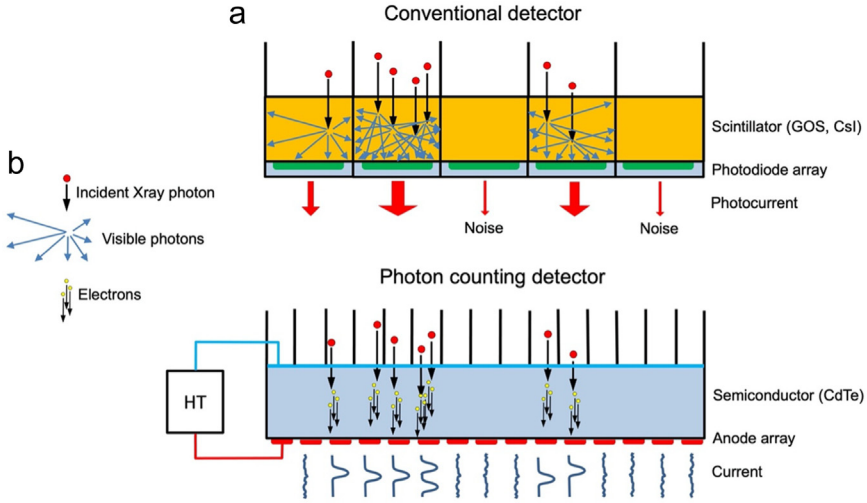


**Figure 1.** Schematic depiction of differences between conventional and photon counting CT detectors. a. This panel shows a conventional detector, in which x-ray photons are converted to visible photons in a scintillator layer, followed by conversion of visible photons into a photocurrent in underlying photodiode array elements. Note the added noise current (present even in the absence of any incident x-rays) and the septa between detector elements needed to limit the lateral travel of visible photons. b. This panel shows a PCD in which there is no scintillator: X-rays release electrons in the semiconductor that are swept to a pixelated anode by an applied HT field. Note the individual output pulses produced by each x-ray photon, absence of septa, and smaller pixel size than that of the conventional detector. CsI, caesium iodide; GOS, gadolinium oxysulphide; HT, high tension. [Color figure can be viewed at www.neuromodulationjournal.org]

**Table 1.** Diagnoses, Targets, and Lead Models for Each Patient.

| Patient | Diagnosis | Target | Leads implanted |
|---|---|---|---|
| A | PD | STN | Boston Scientific Vercise Cartesia X |
| B | PD | STN | Boston Scientific Vercise Cartesia DB-2202-30 |
| C | ET | VIM | Abbott Infinity 6171 |
| D | PD | STN | Boston Scientific Vercise Cartesia DB-2202-30 |
| E | DT | VIM/GPi | Abbott Infinity 6170/6171 |
| F | PD | STN | Medtronic Sensight B33005 |
| G | PD | STN | Boston Scientific Vercise Cartesia DB-2202-30 |
| H | PD | STN/ZI | Boston Scientific Vercise Cartesia DB-2202-30 |
| I | ET | VIM | Abbott Infinity 6171 |
| J | PD | STN | Boston Scientific Vercise Cartesia DB-2202-30 |
| K | PD | STN | Boston Scientific Vercise Cartesia DB-2202-30 |
| L | PD | GPi | Boston Scientific Vercise Cartesia DB-2202-30 |
| M | PD | STN | Boston Scientific Vercise Cartesia DB-2202-30 |
| N | PD/MSA | PPN | Abbott Infinity 6171 |
| O | ET | VIM | Abbott Infinity 6171 |

DT, dystonic tremor; ET, essential tremor; GPi, globus pallidus internus; MSA, multisystem atrophy; PD, Parkinson's disease; PPN, pedunculopontine nucleus; STN, subthalamic nucleus; VIM, ventral intermediate nucleus; ZI, zona incerta.

Medtronic (Minneapolis, MI), Boston Scientific (Marlborough, MA), and Abbott (Austin, TX). This is a retrospective case series review containing no identifiable data, for which formal ethical approval was not required.

### Imaging Protocol

Postoperative CT imaging was performed with a PCD CT scanner (Siemens Naeotom Alpha Version VA50, Siemens Healthineers, Forchheim, Germany). A standard CT brain protocol was used (scan

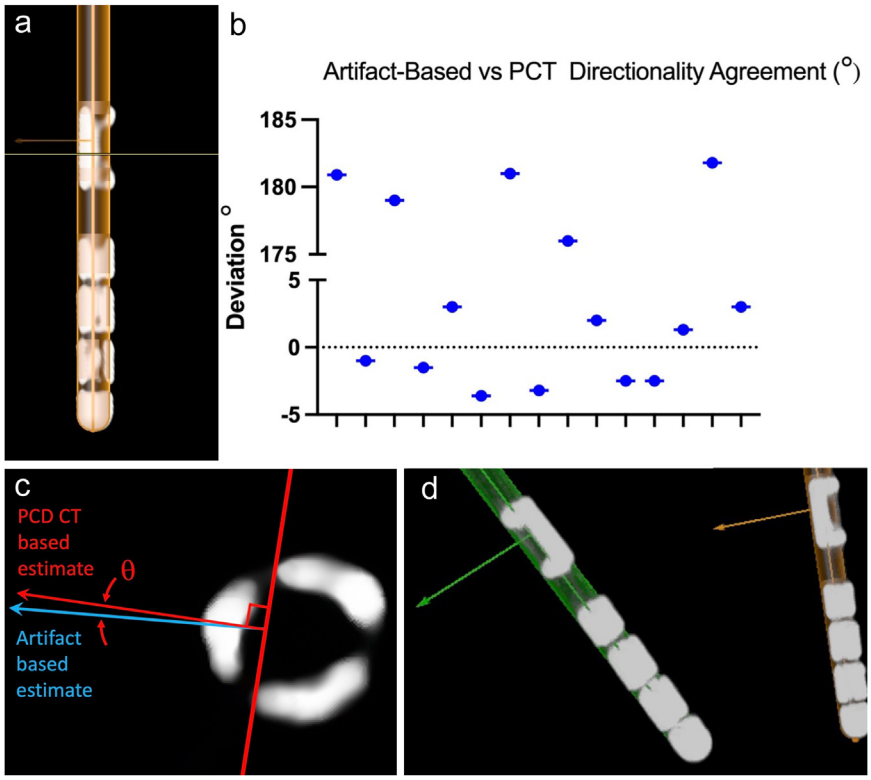


**Figure 2.** Comparison of artifact-based and PCD CT-based lead reconstructions and orientation estimates. a. Reconstruction of a Boston Cartesia 2202 lead based on standard CT artifact analysis, overlaid onto PCD CT wire imaging. The model can be seen to correspond closely to the directly imaged lead. b. Scatter plot of 15 leads comparing the deviation between PCD CT directly measured orientation angles and artifact-based reconstructions. A bimodal distribution is seen with ten of 15 cases corresponding closely and five of 15 deviating by close to 180°. c. The blue arrow represents artifact-based estimation of lead orientation. This was superimposed on a cross section of the lead on PCD CT wire imaging and the red construction lines added to estimate the orientation from the image. The angle θ represents the difference in estimation using the two methods. d. PCD CT 3D wire renderings (maximum intensity projection view), superimposed on artifact-based lead reconstructions. For the orange lead, the orientation assessments agree, but for the green lead, they differ by approximately 180°. [Color figure can be viewed at www.neuromodulationjournal.org]

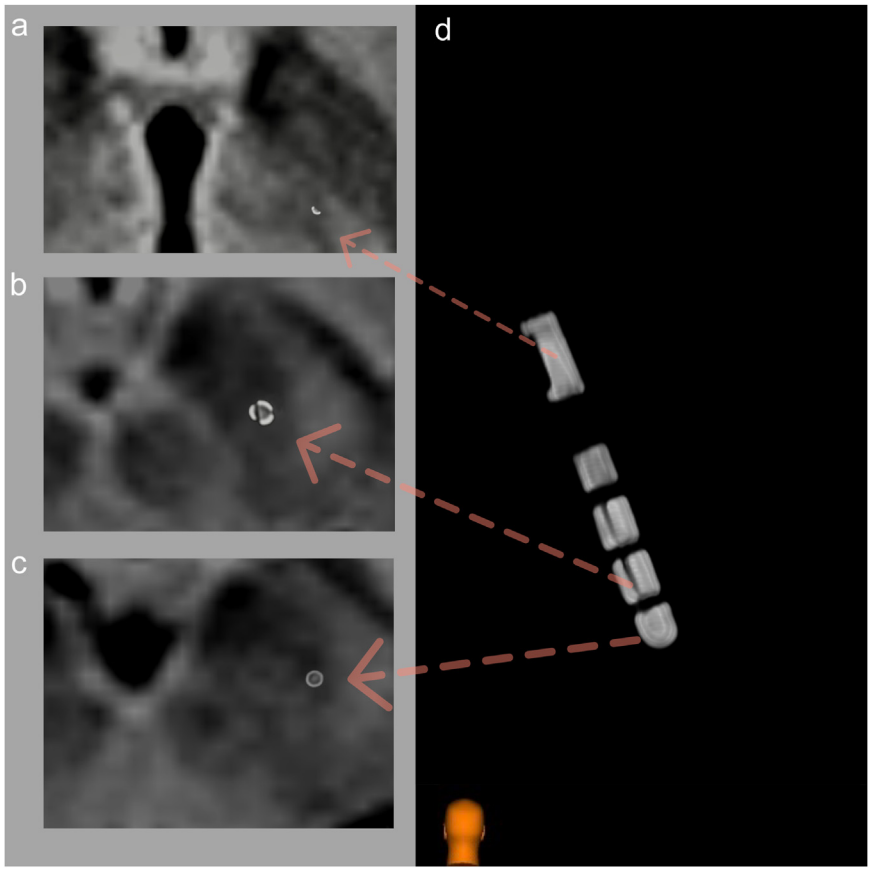


**Figure 3.** Boston Cartesia DB-2202 to subthalamic nucleus target. A 3D rendering of a directional electrode in the left subthalamic nucleus, with corresponding axial slices through directional marker, lower segmented, and ring contacts (all fused to preoperative axial MRI fluid-attenuated inversion recovery [FLAIR]). It can be immediately appreciated, both from the mannequin and the axial slice through the directional marker, that the lead is oriented posteromedially. [Color figure can be viewed at www.neuromodulationjournal.org]

mode: routine spiral adult head quantum plus Xcare; tube voltage: 120 kV; effective mAs 311; acquisition 96 × 0.4 mm volume CT dose index (CTDIvol): 55.7; pitch: 0.35; rotation time (seconds) 0.5; reconstruction slice thickness: 0.6 mm; slice increment: 0.4 mm; reconstruction kernel: HR44; quantum iterative reconstruction [QIR] strength: 3; matrix size: 512 × 512), with high-resolution imaging covering the region from the lead tip to just above the orientation marker (scan mode: routine spiral adult head high-resolution ultra quantum plus; tube voltage: 120 kV; detector collimation: 120 × 0.2 mm; image quality level: 150; CTDIvol: 23.2; pitch: 1 (adapted); rotation time (seconds) 1; reconstruction slice thickness: 0.2 mm; slice increment: 0.1 mm; reconstruction kernel: HR98 (adapted for wire tip visualization); QIR strength: 3; matrix size: 1024 × 1024).

The CT images were fused with preoperative 3T magnetic resonance imaging (MRI) scans on a DBS planning workstation (Neuroinspire, Renishaw, Gloucester, UK).

### Dose Comparison

X-ray dose information was collected for all 15 patients. For comparison, radiation dosages from both conventional CT imaging and fluoroscopy for lead orientation were extracted from imaging records for 15 consecutive patients imaged before the introduction of PCD CT.[18]

Dosage data were tested for normality of distribution using the Shapiro-Wilk test. Normally distributed data were compared using unpaired *t*-tests.

### Comparison With Artifact-Based Analysis

Electrode orientation estimates using PCD CT reconstructions were compared with estimates based on CT artifact analysis performed using commercially available software (Elements, Brainlab AG, Munich, Germany). The latter has only been phantom validated using Boston Scientific directional leads[18]; hence, comparisons were restricted to these cases (18 leads from nine cases).

The standard CT brain protocol images (0.8 mm axial reconstruction sequences) were used for artifact-based analysis, and the usual lead autodetection workflow steps followed. The PCD CT high-resolution wire imaging sequences were then uploaded and fused with the standard CT brain sequences, allowing the computed lead reconstructions to be superimposed on the high-resolution wire imaging (Fig. 2a). The artifact analysis software automatically projects an arrow in the computed direction of the lead orientation marker. For the PCD CT estimate, we used a method similar in principle to the "iron-sights" technique that has previously been used with rotational fluoroscopy; for example,[11] on the lead cross section, a line was drawn through the gaps between the contact segment that is on the same side of the lead as the lead orientation marker and the other two segments. This is shown in Figure 2c (red lines). The orientation estimate is given by a line perpendicular to this in the direction of the orientation marker. The angle between the two estimates was then measured with the software's inbuilt angle measuring tool, with a positive angle denoting the automated estimate being further clockwise than the

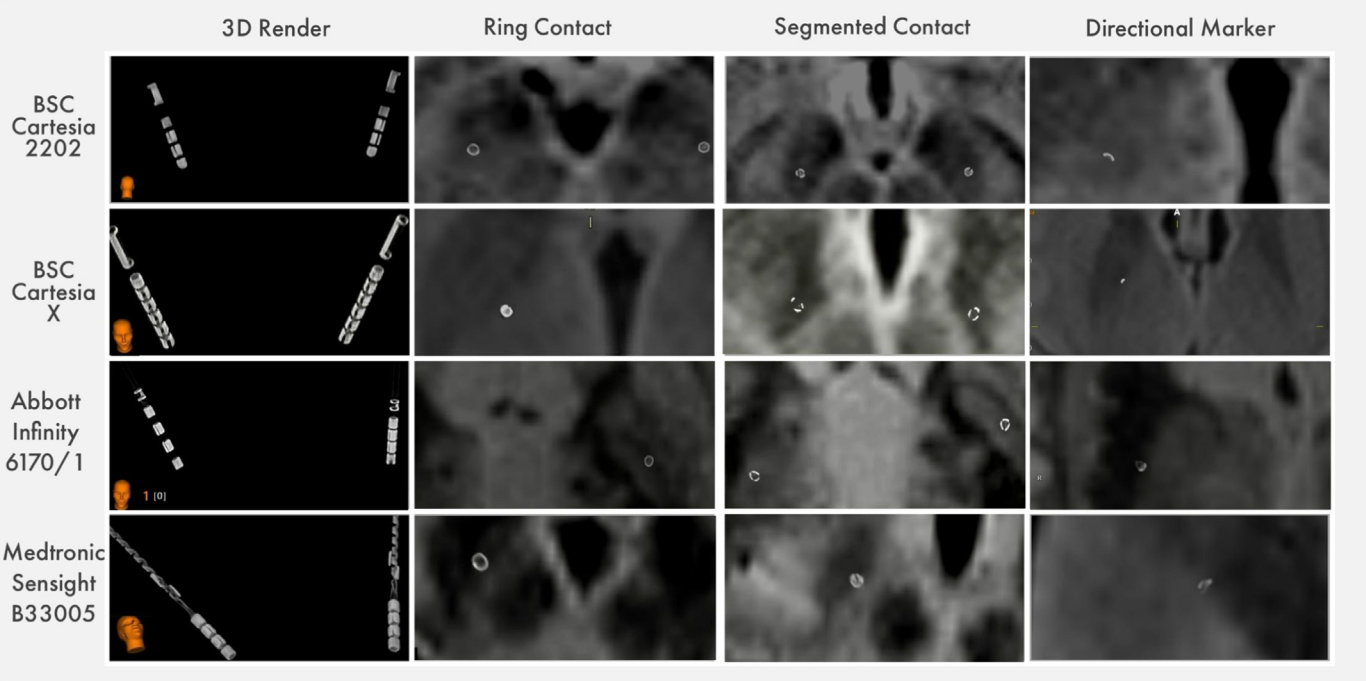


**Figure 4.** Multimanufacturer electrode and contact imaging. This illustration shows PCD CT 3D electrode rendering with orientating mannequin along with axial cuts displaying ring contacts, segmented contacts, and directional orientation markers for four different leads (all coregistered with preoperative axial MRI FLAIR). Note the Medtronic Sensight triangular directional orientation markers with axial cut indicating the vertices of two adjacent triangles. All leads show segmented contacts in the subthalamic nucleus target, except for the Abbott leads, which are in the right ventral intermediate nucleus and left globus pallidus internus. BSC, Boston Scientific. [Color figure can be viewed at www.neuromodulationjournal.org]

PCD CT estimate. Finally, the automated reconstruction was compared with the overlaid CT visualized lead and the longitudinal (depth) discrepancy based on the electrode tip position also measured.

## RESULTS

High-quality images were obtained clearly indicating the directional contacts both on CT and when fused to MRI, as illustrated in Figures 3 to 5.

Mean ionizing radiation dose length products (DLP) for the CT brain and high-resolution electrode imaging were 927 mGy*cm (range 868–1007) and 110 mGy*cm (range 87.5–191) respectively. Individual values are shown in Table 2. Dedicated wire imaging sequences thus accounted for approximately 12% of the total radiation dose. The mean total dose was 1037 mGy*cm. This was normally distributed (Shapiro-Wilk test $p = 0.068$), with a SD of 61.2 mGy*cm.

For the patients who underwent conventional postoperative CT and x-ray fluoroscopy, mean DLP was 1025 mGy*cm (range 876–1176) for CT and 138 mGy*cm (range 76.2–242) for fluoroscopy. Individual values are shown in Table 3. Mean patient total radiation dose (CT + fluoroscopy) was 1162 mGy*cm. This also was normally distributed (Shapiro-Wilk test $p = 0.98$) with a SD of 87 mGy*cm and significantly higher by approximately 12% than the equivalent mean total dose of PCD CT with wire imaging (unpaired $t$-test $p = 0.0001$). PCD CT doses alone (ie, without wire imaging) also were significantly lower by approximately 10% than those of conventional CT alone (unpaired $t$-test $p = 0.0006$).

Concordance of orientation estimation, between direct measurement on PCD CT and artifact-based software analysis, was assessable for 15 of 18 Boston Scientific leads. For the other three leads, no automated estimation was possible owing to excessive polar angle between lead and scanner axis (>55°). The results of the comparison were bimodally distributed (Fig. 2b). In ten cases, measured deviations ranged from −3.6° to +3° with mean −0.50° (SD 2.59°). In the remaining five cases, measured discrepancies ranged from 176° to 181.8° (mean 180°, SD 2.33°). An example of an approximately 180° discrepancy is shown in Figure 2d (lead on left side of image). Longitudinal (depth) deviation between the tip of the reconstructed lead against the visualized lead tip overlay (Fig. 2a) ranged from −1 mm to 0.5 mm with a mean discrepancy −0.05 mm (SD 0.40 mm).

We found that the electrode contacts across the three manufacturers could be adequately appreciated with consistent windowing and level settings on our planning station (Table 4). We then made further adjustments to the image window level and width to resolve the internal wiring components within the leads, with a view to potential use for fault finding in cases of suspected lead fracture. The window settings that were found optimal for these are listed in Table 4. There are significant differences in lead construction among manufacturers, which affected the ability to resolve internal structure. In Boston Scientific and Abbott leads, the wiring to each contact runs in a separate lumen within the plastic of the lead, and this provides sufficient separation between the wires for them to be individually resolved. The Medtronic lead is constructed differently and contains a structure resembling a helically coiled ribbon cable. To date, we have been unable to resolve the individual conductors within this owing to their closer spacing. Imaging of the conductors is presented in Figure 6.

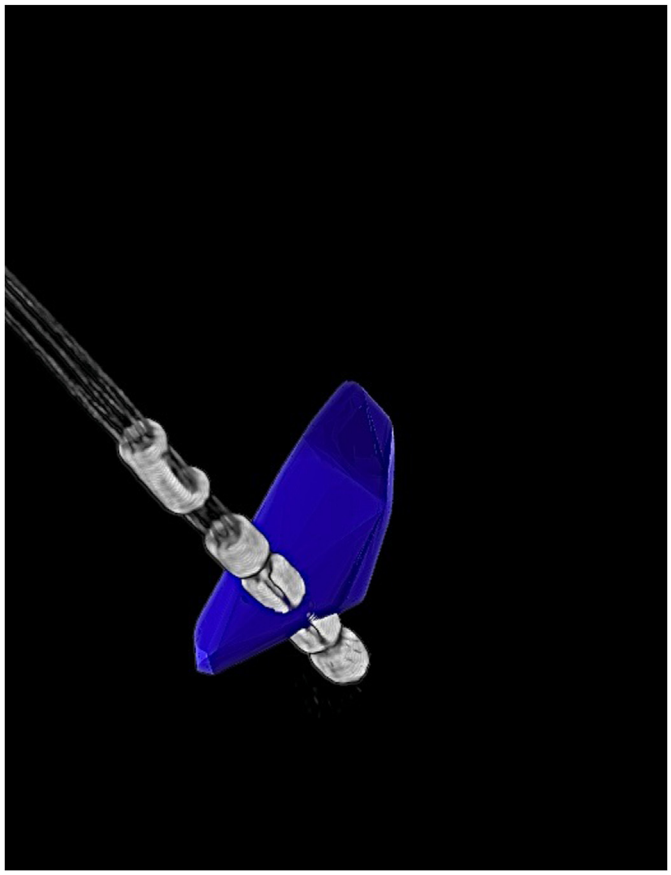

**Figure 5.** Boston Cartesia DB-2202 with segmented subthalamic nucleus figure. Postero-superior view: The segmented contacts and their relationship to the STN (constructed from preoperative MRI FLAIR) can be readily appreciated and so easily used to anatomically optimize programming parameters. [Color figure can be viewed at www.neuromodulationjournal.org]

## DISCUSSION

We have shown how commercially available PCD CT can clearly image directional DBS electrode contacts and orientation markers across manufacturers. Mean DLP ionizing radiation doses for the CT brain and dedicated high-resolution electrode imaging were on average 935 and 110 mGy*cm, respectively. This approximates to effective doses of 1.87 mSv (CT brain) and 0.22 mSv (electrode imaging).[19,20] Despite providing greater imaging detail, the combined dose of both sequences is slightly lower than that of conventional CT brain alone, typically approximately 2.1 to 2.3 mSv[12,21,22] in the literature, and 2.05 mSv (DLP 1025 mGy*cm) in our internal comparator cases. Three-dimensional rotational fluoroscopy adds another approximately 0.2 mSv or more to conventional imaging[11,23] as per the literature, with our comparator group's dose area product of 138 mGy*m$^2$ approximating to 0.179 mSv. Overall, we found the PCD CT, including high-resolution lead tip imaging, delivered a statistically significant 13% dose reduction compared with our previously used combination of standard head CT plus fluoroscopy for lead orientation determination. It is noteworthy that this was achieved despite the PCD slice thickness being 0.4 mm, in contrast to 0.6 mm slices on conventional CT. Had the conventional CT imaging been performed with equivalent slices, the necessary dose would have inevitably been higher.[24]

Commonly used imaging techniques for directional contact orientation evaluation all have limitations. We previously used antero-posterior (AP) and lateral skull radiographs. These have been estimated to have an accuracy of at best 9.5°.[11] Our experience has been that lateral views are frequently difficult to interpret because the images of the two leads overlap, and a degree of image obliquity is required to separate the images, meaning that the AP and "lateral" views are not truly orthogonal; this is likely to degrade accuracy of orientation estimation. To complicate matters further, studies have found small differences between the orientation angles of the direction marker and the segmented electrodes—attributed to deviations within the tolerances of the

**Table 2.** PCD CT Radiation Dosimetry (DLP in mGy*cm)

| Patient | CT head DLP | Wire imaging DLP | Total DLP |
|---|---|---|---|
| A | 909 | 87.5 | 997 |
| B | 1002 | 191 | 1193 |
| C | 947 | 98 | 1045 |
| D | 916 | 126 | 1042 |
| E | 943 | 115 | 1058 |
| F | 926 | 106 | 1032 |
| G | 868 | 116 | 984 |
| H | 907 | 90 | 997 |
| I | 1007 | 104 | 1111 |
| J | 892 | 94 | 986 |
| K | 988 | 106 | 1094 |
| L | 868 | 96 | 964 |
| M | 887 | 106 | 993 |
| N | 964 | 105 | 1069 |
| O | 886 | 108 | 994 |
| Mean | 927 | 110 | 1037 |

**Table 3.** Radiation Dosimetry for Conventional CT With Fluoroscopy (DLP in mGy*cm).

| Patient | CT head DLP | Fluoroscopy DLP | Total DLP |
|---|---|---|---|
| AA | 1064 | 76.2 | 1140 |
| BB | 1175.8 | 91.3 | 1267 |
| CC | 875.8 | 165.2 | 1041 |
| DD | 1056.1 | 128 | 1184 |
| EE | 1055.9 | 151 | 1207 |
| FF | 909.9 | 168 | 1078 |
| GG | 917 | 77 | 994 |
| HH | 973 | 197 | 1170 |
| II | 1127 | 184.4 | 1311 |
| JJ | 994 | 138.5 | 1133 |
| KK | 1037 | 131.4 | 1168 |
| LL | 1032 | 68.6 | 1101 |
| MM | 1045 | 113 | 1158 |
| NN | 1038 | 241.6 | 1280 |
| OO | 1071 | 136.4 | 1207 |
| Mean | 1025 | 138 | 1163 |

**Table 4.** Typical Windowing Settings for Electrode Contact and Internal Wiring Component Visualization.

| Object of interest | Level | Width |
|---|---|---|
| Electrode contact | 40000 | 70000 |
| Internal Wiring | 35000 | 70000 |

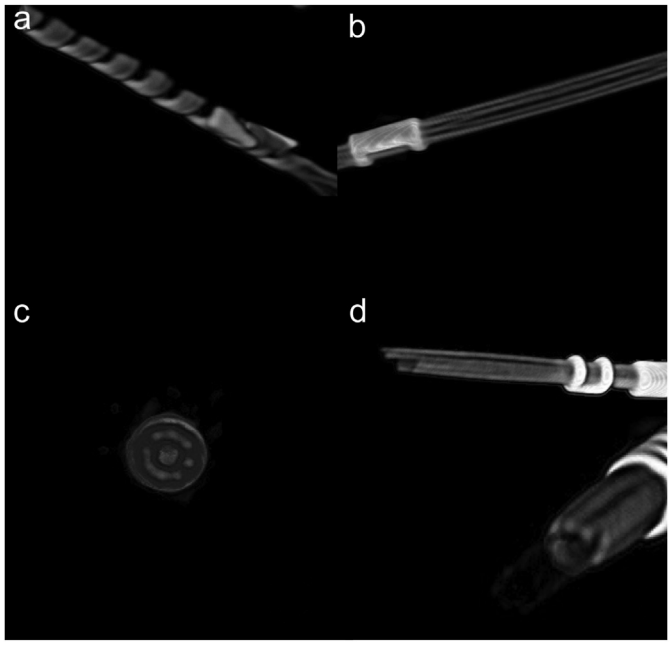


**Figure 6.** Electrode wire imaging. a. Medtronic Sensight B33005. b. and c. Boston Cartesia DB-2202-30 (panel c is a cross section of the lead). d. Abbott Infinity 6170/6171. Although the Medtronic lead has a construction resembling a spirally wound ribbon cable, in the Abbott and Boston Scientific leads, the individual wires are well separated and can be resolved individually.

handmade lead assembly process.[10,12,25] The iron sights technique[11,12] is a more accurate method by which rotational fluoroscopy is used to find an angle where a radiolucent gap is visualized in a segmented electrode, owing to the alignment of a line connecting two of the gaps between electrode segments with the x-ray beam. Nevertheless, to fully delineate directional electrode orientation requires three angles: not just rotation about the lead axis but also two tilt angles.[12,26]

Algorithms have been developed to extract electrode orientation information from CT images on the basis of analysis of streak artifact.[10,18] These require a polar angle between the lead and the scanner axis of <40° to 55° to ensure sufficient artifact for analysis, and they may still miscalculate by 180° owing to artifactual symmetry[18,27]—thus needing additional confirmatory imaging (for instance, with AP and lateral radiographs) to disambiguate the two possible solutions. Our findings are consistent with these previously described limitations of artifact-based reconstructive algorithms: Of 18 electrodes, three were not assessable by the automated software owing to insufficient angle between lead and scanner axis, and for five leads, the artifact-based estimate was approximately 180° in error. For the remaining ten leads, agreement was very close between direct CT imaging and artifact-based estimation, for both orientation and depth. Although software refinement is ongoing, reconstructive validation is restricted to specific proprietary electrode brands on certain CT scanners, and the techniques are accordingly not yet universally generalizable.[10,18]

Direct visualization as shown here enables unambiguous determination of the precise electrode-contact orientation regarding to the functional environment to facilitate tailored directional steering. Postoperative CT imaging is already routinely obtained in many DBS centers for both target accuracy confirmation and hematoma exclusion.[10] By streamlining our workflow to obtain a single postoperative PCD CT, we have obviated the need for radiographs and facilitated anatomically guided programming from the outset. The programming clinician can easily generate a hypothesis as to the most promising contacts on the basis of a simple fusion and direct visualization, without recourse to more involved reconstructions with uncertainties remaining regarding their accuracy.

At present, many units only attempt directional programming if issues are encountered after a conventional omnidirectional monopolar-review programming trial delivered to the entire ring.[3,5] The challenges of ascertaining exact contact orientation and the labor-intensiveness of a trial-and-error programming strategy can lead to an understandable reticence to explore directionality first line. This may mean that the full potential benefits of directionality concerning optimized therapeutic window, patient, and clinical preference and IPG longevity remain incompletely exploited. Imaging-guided anatomically based programming has been shown to significantly reduce programming time, by 56% in one recent study,[6] and future studies could address whether such an approach combined with photon-counting CT imaging may yield further benefit.

An unexpected benefit of the high-resolution imaging was the ability in some cases to resolve internal lead structure, specifically the wiring leading to each contact. Applying high-resolution imaging to the extracranial part of the lead under the scalp may prove useful in situations of suspected lead fracture, for example, after a blow to the scalp, particularly those in which some but not all impedances are high so that a visible macroscopic fracture might not be expected on plain x-ray.

PCD-equipped CT scanners are not yet commonplace, and not all DBS centers will have access to them at present. PCDs unfortunately cannot be retrofitted to existing machines. However, this technology is showing benefits in a wide range of clinical settings owing to improved imaging quality, absence of noise, and decreased radiation and contrast agent doses. Food and Drug Administration clearance was obtained in September 2021. At the time of writing, there are published articles referencing PCD CT from 15 countries in Europe, North America, and Australasia. Promising applications include breast and cardiovascular imaging in which small vessel examinations are presently hampered by limited spatial resolution[14]; for instance, in PCD CT coronary arteriography, arterial plaques can be unambiguously distinguished from luminal contrast.[15] Thus, although access to PCD CT is limited for now, it is sure to increase rapidly, and we envisage that this kind of direct electrode visualization will become routine in the next few years. More work is needed in future to assess the influence of the method on clinical outcomes.

## CONCLUSIONS

We show in the present study that photon-counting CT can readily image DBS electrode directional segmentation for all major commercially available systems while reducing radiation exposure compared with conventional imaging. This obviates the need for more complex and labor-intensive techniques to assess directional orientation, which are themselves not without limitations.

### Authorship Statements

James Manfield and James J. FitzGerald conceived the project; James Manfield drafted the manuscript and collected and collated

data; James Manfield and James J. FitzGerald analyzed data, with important intellectual input from Alexander L. Green, Nagaraja Sarangmat, and Marko Bogdanovic. Sheena Thomas and Charalambos Antoniades facilitated the imaging including protocol optimization. All authors critically revised the manuscript.

## Conflict of interest

Alexander L. Green reports consulting fees from Abbott and has received travel support from Medtronic, Boston Scientific, and Abbott. James J. FitzGerald reports consulting fees from Abbott and Boston Scientific and has participated on data safety monitoring boards for Medtronic and Herantis. James Manfield reports travel support from Boston Scientific and Abbott. Nagaraja Sarangmat has received travel support from Medtronic and Boston Scientific. The remaining authors reported no conflict of interest.

**How to Cite This Article**

Manfield J., Thomas S., Bogdanovic M., Sarangmat N., Antoniades C., Green A.L., FitzGerald J.J. 2024. Seeing Is Believing: Photon Counting Computed Tomography Clearly Images Directional Deep Brain Stimulation Lead Segments and Markers After Implantation. Neuromodulation 2024; 27: 557–564.

## REFERENCES

1. Karl JA, Joyce J, Ouyang B, Verhagen Metman L. Long-term clinical experience with directional deep brain stimulation programming: a retrospective review. *Neurol Ther*. 2022;11:1309–1318.
2. Schnitzler A, Mir P, Brodsky MA, et al. Directional deep brain stimulation for Parkinson's disease: results of an international crossover study with randomized, double-blind primary endpoint. *Neuromodulation*. 2022;25:817–828.
3. Merola A, Romagnolo A, Krishna V, et al. Current directions in deep brain stimulation for Parkinson's disease-directing current to maximize clinical benefit. *Neurol Ther*. 2020;9:25–41.
4. Rammo RA, Ozinga SJ, White A, et al. Directional stimulation in Parkinson's disease and essential tremor: the Cleveland Clinic experience. *Neuromodulation*. 2022;25:829–835.
5. Schüpbach WMM, Chabardes S, Matthies C, et al. Directional leads for deep brain stimulation: opportunities and challenges. *Mov Disord*. 2017;32:1371–1375.
6. Lange F, Steigerwald F, Malzacher T, et al. Reduced programming time and strong symptom control even in chronic course through imaging-based DBS programming. *Front Neurol*. 2021;12, 785529.
7. Lange F, Steigerwald F, Engel D, et al. Longitudinal assessment of rotation angles after implantation of directional deep brain stimulation leads. *Stereotact Funct Neurosurg*. 2021;99:150–158.
8. Dembek TA, Hoevels M, Hellerbach A, et al. Directional DBS leads show large deviations from their intended implantation orientation. *Parkinsonism Relat Disord*. 2019;67:117–121.
9. Dembek TA, Asendorf AL, Wirths J, Barbe MT, Visser-Vandewalle V, Treuer H. Temporal stability of lead orientation in directional deep brain stimulation. *Stereotact Funct Neurosurg*. 2021;99:167–170.
10. Hellerbach A, Dembek TA, Hoevels M, et al. DiODe: directional orientation detection of segmented deep brain stimulation leads: a sequential algorithm based on CT imaging. *Stereotact Funct Neurosurg*. 2018;96:335–341.
11. Reinacher PC, Krüger MT, Coenen VA, et al. Determining the orientation of directional deep brain stimulation electrodes using 3D rotational fluoroscopy. *AJNR Am J Neuroradiol*. 2017;38:1111–1116.
12. Egger K, Rau A, Urbach H, Reisert M, Reinacher PC. 3D X-ray based visualization of directional deep brain stimulation lead orientation. *J Neuroradiol*. 2022;49:293–297.
13. Willemink MJ, Persson M, Pourmorteza A, Pelc NJ, Fleischmann D. Photon-counting CT: technical principles and clinical prospects. *Radiology*. 2018;289:293–312.
14. Flohr T, Petersilka M, Henning A, Ulzheimer S, Ferda J, Schmidt B. Photon-counting CT review. *Phys Med*. 2020;79:126–136.
15. Kreisler B. Photon counting Detectors: concept, technical challenges, and clinical outlook. *Eur J Radiol*. 2022;149:110229.
16. Lin E, Alessio A. What are the basic concepts of temporal, contrast, and spatial resolution in cardiac CT? *J Cardiovasc Comput Tomogr*. 2009;3:403–408.
17. Kakinuma R, Moriyama N, Muramatsu Y, et al. Ultra-high-resolution computed tomography of the lung: image quality of a prototype scanner. *PLoS One*. 2015;10, e0137165.
18. Dembek TA, Hellerbach A, Jergas H, et al. DiODe v2: unambiguous and fully-automated detection of directional DBS lead orientation. *Brain Sci*. 2021;11:1450.
19. McCollough C, Cody D, Edyvean S, et al. Report No. 096 - the measurement, reporting, and management of radiation dose in CT. *American Association of Physicists in Medicine*. 2008;23:1–28.
20. Shrimpton PC, Jansen JT, Harrison JD. Updated estimates of typical effective doses for common CT examinations in the UK following the 2011 national review. *Br J Radiol*. 2016;89, 20150346.
21. Manninen AL, Isokangas JM, Karttunen A, Siniluoto T, Nieminen MT. A comparison of radiation exposure between diagnostic CTA and DSA examinations of cerebral and cervicocerebral vessels. *AJNR Am J Neuroradiol*. 2012;33:2038–2042.
22. Smith-Bindman R, Lipson J, Marcus R, et al. Radiation dose associated with common computed tomography examinations and the associated lifetime attributable risk of cancer. *Arch Intern Med*. 2009;169:2078–2086.
23. Bridcut RR, Murphy E, Workman A, Flynn P, Winder RJ. Patient dose from 3D rotational neurovascular studies. *Br J Radiol*. 2007;80:362–366.
24. Raman SP, Mahesh M, Blasko RV, Fishman EK. CT scan parameters and radiation dose: practical advice for radiologists. *J Am Coll Radiol*. 2013;10:840–846.
25. Husch A, V Petersen MV, Gemmar P, Goncalves J, Hertel F. PaCER-A fully automated method for electrode trajectory and contact reconstruction in deep brain stimulation. *NeuroImage Clin*. 2018;17:80–89.
26. Treuer H, Hellerbach A, Borggrefe J, Visser-Vandewalle V. Regarding "determining the orientation of directional deep brain stimulation electrodes using 3D rotational fluoroscopy". *AJNR Am J Neuroradiol*. 2017;38.
27. Kurtev-Rittstieg R, Achatz S, Nourinia A, Mittermeyer S. Orientation of directional deep brain stimulation leads on CT: resolving the ambiguity. *bioRxiv*. Preprint posted online September 18, 2020. https://doi.org/10.1101/2020.09.16.298653

## COMMENT

The authors of this study offer an excellent solution to determination of the "directionality" of the recently introduced directional DBS leads. Using a novel imaging modality—the PCD CT—they were able to "see" the separation between directional DBS electrode contacts and the exact position of the directional marker, and therefore establish the three-dimensional direction of the split electrodes. Looking at the illustrations of the article, the difference in image resolution is quite obvious, and the next question would be whether such imaging is readily available worldwide (or at least in neurosurgical centers that specialize in DBS surgery). After reading this article, I will be inquiring from my radiology colleagues whether PCD CT is available in our city so we can use it in our patients for postoperative verification and subsequent troubleshooting. However, despite the inevitable enthusiasm, PCD CT is still a radiologic x-ray–based test that requires special equipment and exposes patients to ionizing radiation, whereas ideally, this verification should be performed through a completely safe evaluation, preferably with a portable device. An analogy with programmable shunts comes to mind: In the beginning, radiographs were the only way to check the shunt setting, but now, the settings are tested with a compass-like contraption or an electromagnetic "reader." I am therefore optimistic that soon, there will be a different way to check the electrode type, depth, and direction, and that the ingenious spirit of the DBS community will not rest until such a way is developed.

Konstantin Slavin, MD
*Chicago, IL, USA*